Anomalous Anderson transition in carbonized ion-implanted polymer *p*-phenylenebenzobisoxazole

G. Du* and A. Burns†
Department of Physics, The Ohio State University, Columbus, Ohio 43210-1106

V. N. Prigodin
Department of Physics, The Ohio State University, Columbus, Ohio 43210-1106
and A. F. Ioffe Physico-Technical Institute, 194021 St. Petersburg, Russia

C. S. Wang
University of Dayton Research Institute, Dayton, Ohio 45469

J. Joo‡
Department of Physics, The Ohio State University, Columbus, Ohio 43210-1106

A. J. Epstein
Department of Physics and Department of Chemistry, The Ohio State University, Columbus, Ohio 43210-1106
(Received 26 August 1999)

We report a charge transport study which revealed an unusual insulator-metal transition in ion implanted polymer *p*-phenylenebenzobisoxazole. Upon ion implantation, a carbonized layer forms on film sample surface and becomes increasingly conductive with increasing ion implantation dosage. A drastic change in the temperature dependence of conductivity $\sigma(T)$ with increasing ion dosage is observed at this transition. The low dosage samples ($\leqslant 7\times10^{16}$ ions/cm^2) have a low temperature insulating conductivity: $\sigma(T)\sim\exp[-(T_0/T)^\gamma]$, where γ was obtained at 0.74 increasing to 1/4 with increasing dosage. To explain the unusual value $\gamma=0.74$, we extend Mott's variable range hopping model by including in the consideration of an energy dependence of density of states near the Fermi level. This model also explains a temperature dependent conductivity near the insulator-metal transition in these low dosage dielectric samples. On the other hand, the high dosage samples ($\geqslant 10^{17}$ ions/cm^2) show a semimetallic conductivity: $\sigma(T)=\sigma_0+\Delta\sigma(T)$, where $\Delta\sigma(T)$ is due to electron-electron interaction and weak localization effects with the latter undergoing a dimensional crossover from three dimensions to two dimensions below $\sim$40–50 K as reported earlier.

I. INTRODUCTION

Carbonaceous materials exhibit a wide range of transport properties. Diamond and graphite are two well known materials at opposite ends. Diamond, consisting of crystalline saturated sp^3 bonding, is an excellent insulator with a room-temperature conductivity $\sigma_{\rm RT}\sim10^{-18}$ S/cm. Graphite, on the other hand consisting of layers of unsaturated and crystalline sp^2 bonding, is metallic with $\sigma_{\rm RT}\sim10^4$ S/cm. Other carbon materials, disordered or with impurities, have various transport properties in between these two forms.[1] For example, high-temperature treated glassy carbons have $\sigma_{\rm RT}\sim10^2$ S/cm with a weak temperature dependent conductivity $\sigma(T)$ and are semimetallic,[2] while most amorphous carbons with $\sigma_{\rm RT}$ up to 10^{-2} S/cm and hopping or tunneling conductivity

$$\sigma(T)=\sigma_1\exp\left[-\left(\frac{T_0}{T}\right)^\gamma\right]\quad(\gamma>0),\tag{1}$$

are insulators.[1]

Other disordered carbonaceous materials studied in recent years include high-temperature annealed polymers with signatures of graphitization upon high-temperature treatment[3] and ion implanted polymers showing similar transport behaviors as amorphous carbons.[4–8] Amorphous carbons have a mixture of sp^3 and sp^2 orbitals. The sp^2 carbons have unpaired π electrons that form a free electron gas in crystalline graphite. It is proposed that more conducting forms such as evaporated or ion beam deposited amorphous carbons ($\sigma_{\rm RT}\sim10^{-2}$ S/cm) have a higher content of sp^2, while less conducting ones such as hydrogenated amorphous carbons ($\sigma_{\rm RT}\sim10^{-6}$ S/cm) have a lower content of sp^2.[1] Therefore, with increasing content of sp^2 states and ordering, a crossover proceeds from an insulating phase in less conductive materials such as amorphous carbons[1] to a semimetallic phase in more conductive ones such as glassy carbons.[2] Such a crossover is similar to an insulator-metal transition (IMT) in doped semiconductors as a function of dopant concentration.[9]

In an earlier paper[10] we reported a comprehensive transport properties of three ion implanted polymers, *p*-phenylenebenzobisoxazole (PBO), *p*-phenylene benzobisthiazole (PBT), and benzimidazobenzophenanthroline (BBL). The first two are rigid rod polymers and the third is a ladder polymer. The results showed that the three high dosage implanted samples are semimetallic with unusual transport properties. Previous studies have shown that the implanted layer of various polymer samples is carbonized to a certain degree depending on the implantation process.[7,8,11]

0163-1829/2000/61(15)/10142(7)/$15.00 PRB 61 10 142 ©2000 The American Physical Society

The incident high energy ions damage the original chemical structure and expel heteroatoms from the polymer systems as revealed by the x-ray photoelectron spectroscopy (XPS) results.[7] Raman scattering studies on implanted PBO (Ref. 7) and other implanted polymers[5] have shown similar C-C bonding similar to that in amorphous carbons, including graphitelike bonding.[12]

It was concluded in our previous report that a three-dimensional interconnected sp^2 rich carbon network reformed upon ion implantation on the densely packed rigid-rod and ladder polymer backbone is responsible for the semimetallic behavior.[10] The unusual behavior includes a dimensional crossover in the weak localization effect from three to two dimensions with decreasing temperature when the Thouless length $L_{Th} \propto T^{p/2}$ $(p>1)$, increasing with decreasing temperature, surpasses the implanted sample thickness.[13,14] This change in dimensionality of localization effect results in an enhanced electron-electron interaction effect at low temperatures, which was observed systematically in other experimental results such as thermoelectric power, magnetoconductance, and microwave dielectric constant.[10]

In the present part of this systematic study, we traced the insulator-metal transition in the implanted PBO samples as a function of implantation dosage. The temperature dependence of $\sigma(T)$ shows a dramatic change, becoming weaker and weaker with increased ion dosage, reflecting an Anderson transition. In addition to the Anderson transition, an unusual result was observed in the temperature dependence $\sigma(T)$ of the most insulating sample. The low dosage samples (φ from 7×10^{15} to 7×10^{16} ions/cm^2) have a general hopping conductivity $\sigma(T) \propto \exp[-(T_0/T)^{\gamma}]$ at low temperatures, where γ were obtained from 0.74 to 1/4 with increasing dosage. The unusual result of $\gamma=0.74$ of the lowest dosage sample is explained in terms of a modification of the band structure due to implantation.

We conclude that the implantation leads first to smearing the sharp edge of the valence band. The Fermi level is also in this smearing region and, therefore, in contrast to traditional dielectrics, the density of states around the Fermi level is energy dependent. Taking into consideration of this energy dependence of the density of states (DOS) near the Fermi energy, we extend the Mott variable range hopping (VRH) model which fits the unusual data. With increasing dosage of samples 2 to 4, the reconstruction of DOS is more pronounced and the DOS becomes a weaker function of energy at the Fermi level, leading to the 3D Mott VRH model $\gamma=1/4$. From fitting we estimated the model parameters for the energy dependent density of states and we have found them to be well self-consistent.

The higher dosage samples (φ from 10^{17} to 10^{18} ions/cm^2) exhibit similar properties to those reported in Ref. 10. The temperature dependence of the conductivity undergoes a dramatic change from the insulating hopping conduction of the lower dosage samples to a semimetallic behavior $\sigma(T)=\sigma_0+\Delta\sigma(T)$ of these higher dosage samples. Thus, an Anderson IMT occurs with increased implantation dosage. The term $\Delta\sigma(T)$ is dominated by the long range electron-electron interaction and weak localization effects.[14] At lower temperatures the weak localization contribution is limited by the thickness of the ion implanted layer ($\sim$1500 Å) leading to a 3D to 2D crossover for this contribution to the conductivity.

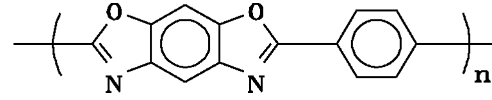

FIG. 1. Chemical structure of polymer PBO.

II. EXPERIMENT

The pristine PBO polymer sample (see Fig. 1) was obtained in the form of biaxial films, free standing and about 50 μm thick (supplied by the Polymer Branch, Materials Directorate, Air Force Research Lab, Dayton, OH). The synthesis and processing of these polymers were published previously.[15] The implantation was performed by a Varian Model 400-AR ion implantor at Honeywell Systems and Research Center, Minneapolis, MN, using 200 KeV $^{84}Kr^{+}$ ions at an ion beam current density of 2 μA/cm^2. Seven ion implantation dosages, from 7×10^{15} to 10^{18} ions/cm^2, were used in this study and are listed in Table I. The implantation process creates a conducting layer $\sim0.15\mu$m thick [estimated by scanning electron microscopy (SEM)] on the film sample surface.[10] The dc conductivity measurements utilized a conventional four probe planar sample configuration with gold wires and silver paint used and the data were taken from a computer controlled current source (Keithley 220) and a multimeter (Keithley 195A). The temperature in this experiment was controlled from 3 to 300 K using liquid helium in a Janis Dewar flask by a LakeShore DRC 82C Temperature Controller and LakeShore DT500 thermosensors. XPS experiments were conducted on both free standing film and spin coated film samples on a Perkin-Elmer Physical Electronics Model 550 ESCA system with Mg Kalpha x-ray source at 1253.6 eV. The pressure was kept below 10^{-8} Torr.

III. RESULTS AND DISCUSSION

A. dc conductivity and the *w* plot

The dc conductivities of the seven implanted PBO samples increase monotonically with increasing ion dosage

TABLE I. The ion dosages φ and the corresponding values of $\sigma_0=\sigma(T\rightarrow0)$, σ_{RT}, and ratio σ_{RT}/σ_{LT} of the seven implanted PBO samples (RT=290 K, LT=4 K for all samples but sample 1 for which LT=22 K since its resistivity was beyond the measurement ability of the instruments below this temperature). A sample thickness $t=0.15$ μm was used in the conductivity calculation. The values of σ_0 for the last three samples are obtained from the fitting of Eq. (7).

Sample No.	φ (ions/cm^2)	σ_0 (S/cm)	σ_{RT} (S/cm)	σ_{RT}/σ_{LT}
1	7×10^{15}	0	2.4	1316
2	1×10^{16}	0	16.4	393
3	4×10^{16}	0	17.2	7.9
4	7×10^{16}	0	25.8	5.4
5	1×10^{17}	93.1	158.6	1.7
6	5×10^{17}	112.9	182.1	1.6
	1×10^{18}	116.3	194.1	1.6

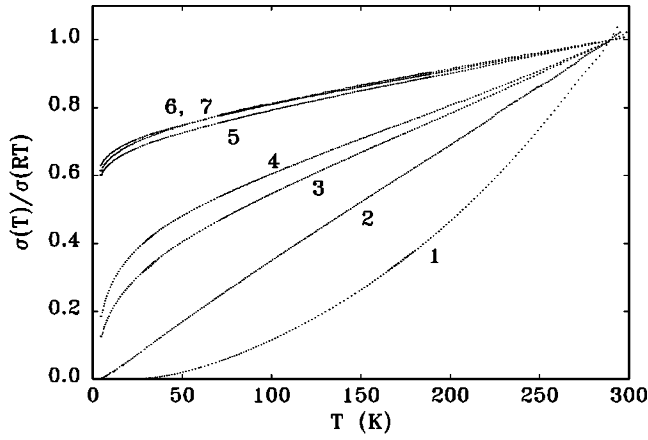

FIG. 2. The normalized conductivities $\sigma(T)/\sigma(290\ \mathrm{K})$ of the seven implanted PBO samples. Note the data for samples 6 and 7 nearly overlap each other. Sample 1 is least conducting, its resistivity was beyond the measurement ability of our instruments below 20 K.

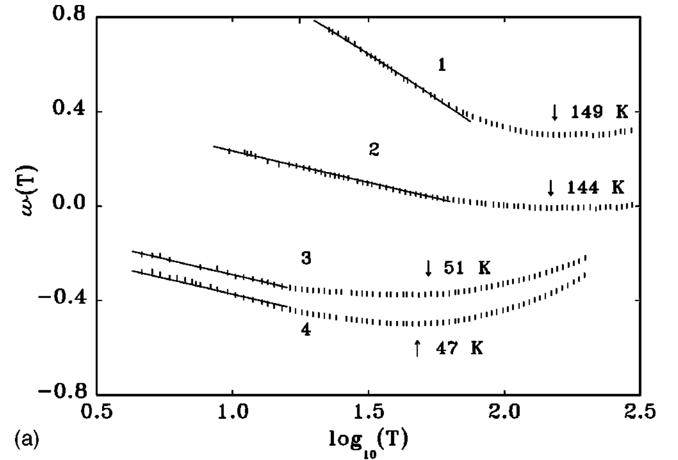

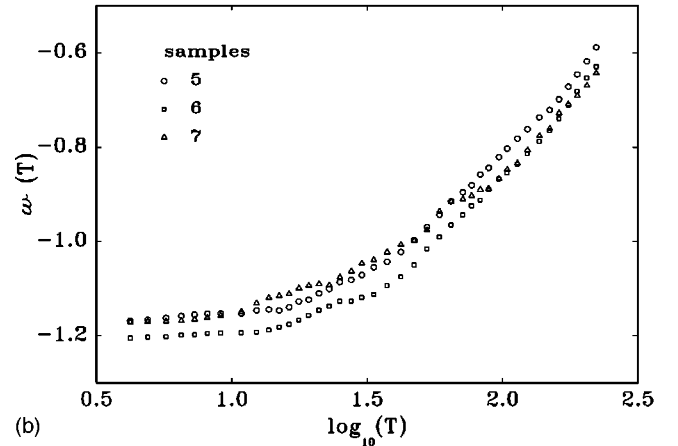

FIG. 3. (a) w plot of samples 1 to 4. The solid line on data curve 1 at low temperatures is a fit to Eq. (6). The solid lines on data curves 2–4 at low temperatures are guide to the eye with a slope $-1/4$, corresponding $\gamma=1/4$. The arrows indicate T_c which separating the w plots from negative slopes to positive slopes. (b) w plots of samples 5 to 7.

φ. The room temperature conductivity results σ_{RT}, RT $=290$ K, of these samples are listed in Table I. The pristine materials are the electrical insulators, chemically stable and mechanically strong. For PBO the insulator gap is about 2.5 eV and $\sigma_{\mathrm{RT}}\sim 10^{-12}$ S/cm.[7] Figure 2 plots the normalized conductivities, $\sigma(T)/\sigma_{\mathrm{RT}}$ of the seven implanted samples. It is obvious that with increased ion dosage from samples 1 to 7, not only the conductivity increases, the temperature dependence of the conductivity also becomes weaker as reflected by the decreasing ratio of room temperature conductivity to low temperature value $\sigma_{\mathrm{RT}}/\sigma_{\mathrm{LT}}$, LT$=4$ K, with increasing ion dosage (Table I).

In order to study the conduction mechanism from the conductivity data, we use the same w plot scheme as in our earlier paper,[10,16] that is, to plot the quantity

$$w(T)=\log_{10}\left(\frac{d\{\ln[\sigma(T)]\}}{d[\ln(T)]}\right) \tag{2}$$

versus $\log_{10}(T)$. For an insulating behavior which has a general form Eq. (1) the w-$\log_{10}(T)$ plot yields a straight line with a negative slope -γ. For example, the activation conduction of semiconductors gives $\gamma=1$ and Mott's VRH conduction gives $\gamma=1/(1+d)$, where d is the sample dimensionality.[17] For a semimetallic behavior with a nonzero conductivity at zero temperature,[14] $\sigma(T)=\sigma_0+\Delta\sigma(T)$, where $\Delta\sigma(T)=aT^{\beta}$, the w plot yields a curve with a positive slope with $a,\beta>0$.

Figure 3 shows the w plots of the seven samples. Even though the temperature dependence of the conductivity changes gradually from curves 1 to 7, the w plots can be separated into two groups. The first four curves of lower dosage samples noticeably have a negative slope at low temperatures [Fig. 3(a)] and the three higher dosage samples have no negative slope in the whole temperature range [Fig. 3(b)]. The negative slope at low temperatures in the w plots suggests that the first four samples follow the general insulating hopping conduction, Eq. (1), in this temperature region, which leads to a zero conductivity at zero temperature. In other words, these samples are Fermi glasses with the Fermi level E_F falling into the strongly localized region as illustrated by Fig. 4(a). In addition, these four w plots also reveals an interesting crossover at T_c with a negative slope below T_c to a positive slope above T_c as indicated by the arrows in Fig. 3(a), suggesting a temperature dependent insulator to metal transition. This behavior and an unusual γ value obtained for curve 1 will be discussed in detail in the following section. For samples 5 to 7, the conductivities are weakly temperature dependent, increasing by less than a factor of 2 from 4 K to room temperature (Table I). In addition, the w plots of these samples show no negative slope over the whole temperature range. As we shall see in Sec. III C, the conductivity of these samples follows $\sigma(T)=\sigma_0+\Delta\sigma(T)$. The nonzero conductivity σ_0 at zero temperature indicates that these samples are not insulators as the first four samples. Therefore, with increasing ion dosage or degree of carbonization, the ion implanted PBO system clearly undergoes an Anderson insulator-metal transition.

B. Low dosage samples

The four low dosage samples exhibited the most interesting behaviors. They are still insulators but their room-

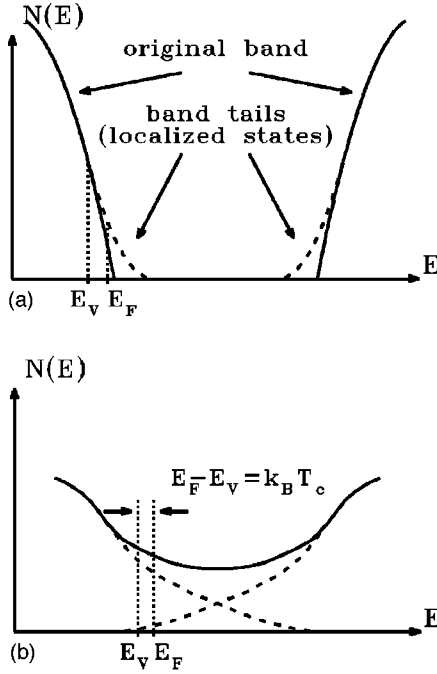

FIG. 4. Fermi glass model. (a) Lightly moderated band structure and (b) strongly moderated band structure.

temperature conductivities are higher than the pristine undoped sample by a factor of $\sim 10^{12}-10^{13}$. This jump in conductivity is assigned to the substantial increase of sp^2 bonding with unpaired π orbitals.[18] These unpaired π electrons may be removed by oxidation. As a result there are acceptor states whose levels are near the top of valence band. The sign of the thermopower confirms that holes are the charge carriers.

In crystalline *p*-doped semiconductors the conductivity follows the Ahrenius law with activation energy which is the energy difference between the acceptor level and the valence band edge. Instead, as we mentioned above, four samples experience a crossover in the slope of the *w* plots from negative at high temperatures to positive at low temperatures. This crossover in *w* plot corresponds in temperature dependent conductivity to a transition from weak almost metallic temperature dependence of conductivity at high temperatures to strong dielectriclike dependence conductivity at low temperatures.

The linear fit of the low temperature *w* plot data of sample 1 yields $\gamma = 0.74$, i.e., $\ln \sigma(T) \propto -T^{-0.74}$. This appreciable deviation from the Ahrenius law indicates that the low-temperature conductivity is not provided only by extended states above the mobility edge, but hopping between the localized states below the mobility edge also contributes to the charge transport. At the same time the value $\gamma = 0.74$ is far from the usually observed Mott numbers[17]: 1/2, 1/3, and 1/3. We note that the Mott conductivity is provided by hopping over localized states uniformly distributed over space and energy.

This unusual temperature dependence can be explained with a modification of the Mott VRH model. The ion irradiation in the implantation process creates disorder in the original polymer structure. According to the Anderson localization theory, such disorder will change the electronic structure of a system.[17] The original sharper band edge will be extended into a smooth band tail where the localized states reside. If the Fermi level is located in the localized region, the system is a Fermi glass (Fig. 4). The four lower dosage samples are apparently examples of Fermi glasses since their conductivity follows the general hopping form of Eq. (1). For a slightly modified band structure, the DOS is close to the original unmodified structure that varies rapidly with energy in the band tail region [Fig. 4(a)]. For a Fermi glass in this case, the Mott assumption[17] of a constant DOS near E_F in deriving the VRH conduction cannot be held. This assumption is especially of concern for sample 1, since the temperature range of interest in this case is finite, thus the energy interval $\delta E = k\,\delta T$ above and below the Fermi level in which the localized states are involved in the hopping conduction is also finite. As a result, the DOS over this energy interval cannot be considered as a constant. We employed an exponentially energy dependent DOS near E_F:[19]

$$N(E) = N_V \exp\left(-\frac{|E-E_V|}{\Delta_0} \right), \tag{3}$$

where E_V is the mobility edge in the valence band and Δ_0 is the scale of the decay of the DOS with $|E_V - E_F| > \Delta_0$, i.e., $N_F \equiv N(E_F) \ll N_V$. For the states over the energy interval δE participating in the transport near the E_F, the average hopping distance $R(\delta E)$ is given by

$$\left[\frac{4\pi}{3} R^3(\delta E) \right]^{-1} = \int_{E_F-\delta E}^{E_F} N(E)\,dE \cong N_F \Delta_0 \exp\left(\frac{\delta E}{\Delta_0} \right), \tag{4}$$

which yields $R(\delta E) = R_F \exp(-\delta E / 3\Delta_0)$, where $R_F = (4\pi N_F \Delta_0 / 3)^{-1/3}$. The hopping conductivity determined by these states is given then

$$\sigma(T) \propto \exp\left[-\frac{\delta E}{T} - \frac{R(\delta E)}{\xi} \right], \tag{5}$$

where ξ is the localization length. Following the Mott procedure of optimizing $\sigma(T)$ over δE, we obtain the *w* function of this conductivity

$$w(T) = p - x + \log_{10}(x+q), \tag{6}$$

where $x = \log_{10} T$, $p = \log_{10}(3\Delta_0)/\log_{10} e$, and $q = -\log_{10} 3\Delta_0 + (|E_V - E_F|/3\Delta_0 \log_{10} e$.

The first term in Eq. (5) corresponds to merely the Ahrenius law and describes the transport of carriers thermally activated at the valence edge. The last term in Eq. (5) represents the difference from the activation law and describes the contribution to the conductivity due to hopping between the exponentially disappearing band tail states. Using Eq. (6), we obtain a good fit to the *w* plot of sample 1 as indicated by the solid line in Fig. 3(a). The optimized fit yields $p = 1.93$ and $q = 0.13$. From *p*, we obtain $3\Delta_0 = 37$ K and using this value with *q*, we obtain $|E_V - E_F| = 145$ K.

It should be noted that this modification only applies to finite temperatures. At extremely low temperatures, i.e., $\delta T \to 0$, the localized states involved in the hopping conduction are those in the close vicinity of the Fermi level, in which case the Mott constant DOS assumption can apply and one should observe $\gamma = 1/4$.

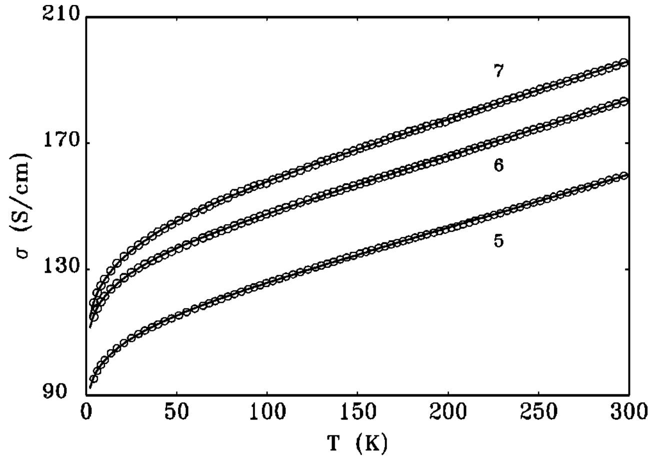

FIG. 5. The sheet conductivities of samples 5–7. Solid lines are fits to Eq. 7 using parameters σ_0, m, B, and c listed in Tables I and II.

For samples 2 to 4, the ion dosages are higher and so is disorder. This will create more localized states into the band tail, which flattens the strongly energy dependent DOS near E_F [Fig. 4(b)]. In this situation the constant DOS can be assumed at the Fermi level, even at finite temperatures. This assertion is supported by the result of $\gamma \cong 1/4$ obtained in this temperature region for these three samples. The solid lines through these three data curves represent linear fittings with $\gamma = 1/4$ [Fig. 3(a)].

Above a characteristic temperature T_c, all four $w(T)$ curves in Fig. 3(a) change to a positive slope, corresponding to a noninsulating phase. Within the Fermi glass model, this crossover can be explained by defining $k_B T_c = |E_V - E_F|$. Therefore, in case of a hole dominated conduction, at $T > T_c$ some electrons will be thermally excited from below E_V, leaving a population of holes in the extended region of the valence band that forms a temperature dependent Fermi liquid [Fig. 4(b)]. As indicated by Fig. 3(a), $T_c \sim 149$ K is obtained for sample 1, which is in an excellent agreement with the value $|E_V - E_F| = 145$ K obtained above.

C. High dosage samples

Samples 5 to 7 have higher conductivities and weaker temperature dependence also becomes weaker as indicated by the small σ_{RT}/σ_{LT} ratio (Table I) and the non-negative slopes of w plots [Fig. 3(b)]. Both these results indicate that these three samples are not insulators as are the first four samples. Their conductivity results are very similar to those of our earlier report.[10] The data very well fit to the semimetallic model developed in Ref. 10

$$\sigma(T) = \sigma_0 + B \ln\left[\sinh\left(\frac{T}{c}\right)^{3/2}\right] + mT^{1/2}, \tag{7}$$

TABLE II. Fitting parameters σ_0, m, B, and c of Eq. (7) for samples 5 to 7. The last two columns are calculated at 300 K.

Sample	m (S/cmK$^{1/2}$)	B (S/cm)	c (K)	$mT^{1/2}/\sigma_0'$	$B'T^{3/2}/\sigma_0'$
5	3.01	0.723	40	0.56	0.16
6	3.21	0.742	40	0.50	0.13
7	3.97	0.753	51	0.59	0.088

where σ_0, a, b, and c are fitting parameters.[10] Figure 5 plots the conductivity results of samples 5 to 7 and the corresponding fitting curves (solid lines) of Eq. (7). The parameters for these curves obtained from nonlinear fitting of the conductivity results using Eq. (7) are listed in Table II.

For $T \gg c$, Eq. (7) becomes

$$\sigma(T) = \sigma_0' + mT^{1/2} + B' T^{3/2}, \tag{8}$$

where $\sigma_0' = \sigma_0 - B \ln(2)$ and $B' = Bc^{-3/2}$. For $T \ll c$, the asymptotic form of Eq. (7) is

$$\sigma(T) = \sigma_0'' + mT^{1/2} + 1.5B \ln(T), \tag{9}$$

where $\sigma_0'' = \sigma_0 - 1.5B \ln(c)$. Equation (8) suggests that at high temperatures the conductivity obtains contributions from a WL effect with phonon-electron scattering as the leading inelastic scattering rate ($T^{3/2}$ term) and an electron-electron interaction effect ($T^{1/2}$ term), both in a three-dimensional case.[14,20] Equation (9) suggests that at low temperatures the WL effect is two dimensional [$\ln(T)$ term],[14,20] while the interaction effect is still three dimensional ($T^{1/2}$ term). The values listed in the last two columns in Table II show that even at RT both WL and electron-electron interaction effects are still approximately first order corrections to σ_0', in accord with the theoretical model.[14,20]

The two asymptotic forms Eqs. (8) and (9) suggest that the WL effect undergoes a dimensional crossover between 4 K and RT whereas the electron-electron interaction effect remains 3D over the whole temperature range. This crossover can be understood by comparing the data with the theoretical predictions. The WL effect for a 3D case is given by

$$\Delta \sigma_L^{3D}(T) = \frac{e^2}{2\pi^2 \hbar L_{Th}}, \tag{10}$$

where Thouless length is given by $L_{Th} = (D\tau_{in})^{1/2}$, D is the diffusion constant and $\tau_{in} \propto T^{-p}$, $p > 1$, is the inelastic scattering time. The Thouless length is used to judge the dimensionality of the WL effect in a system.[14] For an electronically thick of 3D system, one has $L_{Th} < t$ (t is the system thickness); but if $L_{Th} > t$, the system is electronically thin and 2D for the WL effect. For a 2D case,

$$\Delta \sigma_L^{2D}(T) = \frac{\alpha p e^2}{2\pi^2 \hbar} \ln(T), \tag{11}$$

where α should be unity.[14] The electron-electron interaction effect for a 3D case is given by

$$\Delta \sigma_I^{3D}(T) = \frac{e^2}{4\pi^2 \hbar} \frac{1.3}{\sqrt{2}} \left(\frac{4}{3} - \frac{3}{2}F\right) \sqrt{\frac{k_B T}{\hbar D}}, \tag{12}$$

where F is the screening factor.[14]

By comparing the corresponding temperature dependent terms of Eqs. 8 and 9 with those of $\Delta\sigma_L^{3D}, \Delta\sigma_L^{2D}$, and $\Delta\sigma_I^{3D}$, a group of parameters are obtained and listed in Table III (using sample thickness 0.15μm when necessary). As one can see from the table, the value of α is very close to the predicted unity. The dimensional crossover occurs at $T_s \sim 40$ K, reasonably close to value of c given in Table II, at which the Thouless length equals the sample thickness,

TABLE III. Values of $L_{\mathrm{Th}}, T_s, D_m, L_c, \alpha$ obtained from the fitting parameters of Fig. 4. T_s is the temperature at which the Thouless length L_{Th} equals the sample thickness. D_m is the upper limit for the diffusion constant calculated from $\Delta\sigma_I^{3\mathrm{D}}$, assuming the screening factor $F=0$. $L_c=(\hbar D_m/k_BT)^{1/2}$ is calculated at 3 K.

Sample	L_{Th} (m)	T_s (K)	D_m(cm^2/s)	L_c(3 K) (Å)	α
5	$4.3\times10^{-5}T^{-3/2}$	43.6	0.82	145	1.03
6	$4.2\times10^{-5}T^{-3/2}$	42.8	0.72	136	1.05
7	$6.0\times10^{-5}T^{-3/2}$	54.0	0.47	110	1.07

marking the crossover from 3D ($T>T_s$) to 2D ($T<T_s$) for the WL effect. On the other hand, the critical length to judge the dimensionality of the electron-electron interaction effect $L_c=(\hbar D/k_BT)^{1/2}$ (Ref. 14) at $T=4$ K is less than 200 Å for all three samples and much less than the sample thickness (~1500 Å). Thus, the interaction effect is 3D over the whole temperature range. Another result from fitting of Eq. (7) is $p=3$, by comparing the temperature dependence of Eq. (10) and the $T^{3/2}$ term of Eq. (8). This value indicates that the inelastic scattering rate in these samples is dominated by electron-phonon scattering[14] instead of usually observed $p=2$ for electron-electron scattering in a clean limit or $p=3/2$ for electron-electron scattering in a dirty limit in doped semiconductors.[21–23] This result is consistent with the amorphous nature of these implanted polymers. In such a highly disordered system, one would expect electron-phonon scattering dominates electron-electron scattering. All these results show that the model of Eq. (7) is self-consistent and the corresponding discussions in our earlier paper on the properties of this semimetallic phase applies to these samples.

D. Reformed carbon network, IMT, and XPS results

As concluded in our previous paper, the semimetallic behavior of the high dosage implanted samples is due to a reformed 3D interconnected carbon network upon ion implantation on the densely packed pristine samples. This reformed carbon network contains quasi-planar patches of sp^2 rich graphitelike structures and is interrupted three dimensionally by randomly distributed sp^3 sites. The overlap between adjacent extended wave functions from the neighboring graphitelike structures is strong enough for the delocalized π electrons to percolate through the entire sample. This model explains that at higher temperatures, when the Thouless length is smaller than the sample thickness, the samples are 3D for the WL effect; while at low temperatures, the samples are electronically thin when the increasing Thouless length surpasses the sample thickness even though the structure is 3D in nature. The smaller $\sigma^{3\mathrm{D}}(T\rightarrow0)$ indicates that these carbonized systems are just over the insulator-metal transition boundary into the metallic side. In other words, the Fermi energy E_F just passes the mobility edge E_V and locates into the extended state region. As a result, these systems have fewer extended electrons, or a smaller conduction electron density, than the more metallic systems. This result is consistent with the fitting result of $p=3$ indicating electron-phonon scattering dominating the inelastic scattering rate in these materials. For highly disordered systems such as these samples with a small free electron population, electron-phonon scattering is likely to dominate electron-electron scattering.

In lower dosage implantation PBO samples, one obtains insulating behaviors at low temperatures instead. The observed conductivity results of these implanted polymer samples also provide support for the above model, when compared with earlier studied ion implanted polymers. Several groups reported result of $\gamma=1/2$ in the insulating conductivity Eq. (1) and explained it in terms of quasi-1D VRH or tunneling.[5,6,24] In this study, in the temperature region that Eq. (1) was observed, $\gamma=1/4$ or $\gamma=0.74$ were obtained. As shown in Sec. III B, the latter behavior was explained in term of a modified Mott's VRH model. This result, together with the observation of $\gamma=1/4$, suggests that the structure of these implanted samples is three dimensional in nature. Therefore, these systems are structurally different from the early studied implanted polymers which showed either one dimensional behavior or tunneling behavior. What underlines this difference is the densely packed pristine polymer backbone[25,26] in these ladder and rigid rod polymers which provides a basis for the reformed 3D interconnected carbon network. At higher dosages, the extended degree of carbonization leads to a sp^2 rich carbon network and a semimetallic phase in these samples; while at low dosages, a less carbonized system with more impurities (in case of implanted PBO, they are nitrogen and oxygen atoms) results in an insulating

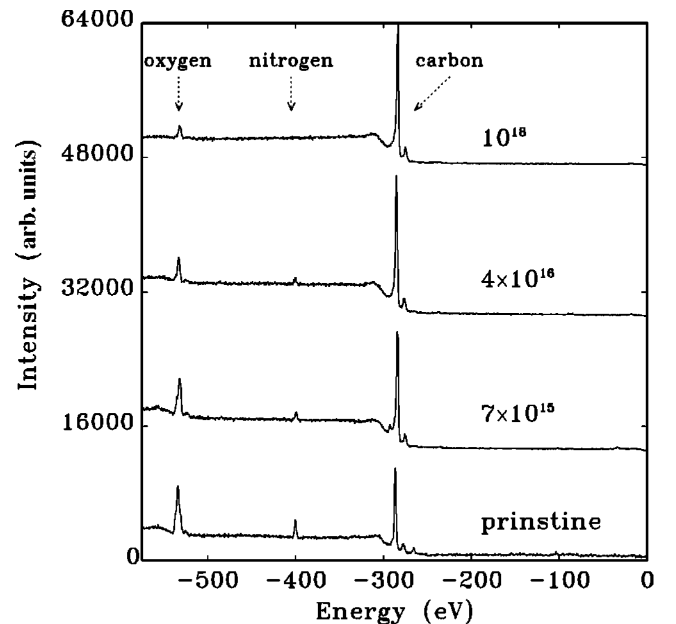

FIG. 6. XPS spectra of implanted PBO samples at different ion dosages.

phase. This change in degree of carbonization as a function of implantation dosage, which leads to the IMT, can be seen clearly in the XPS results. Figure 6 plots the XPS spectra of the implanted PBO samples at different ion dosages. It is obvious that with increasing dosage, the carbon peak intensifies while nitrogen and oxygen peaks reduce greatly, which indicates an increasing degree of carbonization with increasing ion dosage.

IV. CONCLUSION

In summary, we observed an implantation induced Anderson insulator to metal transition in ion implanted polymer PBO as a function of the implantation dosage or degree of carbonization in the system. The lowest dosage sample ($\varphi = 7\times10^{15}$ ions/cm^2) showed an anomalous conductivity attributed to hopping in the tail of the strongly energy dependent DOS. The other low dosage samples ($\varphi \leqslant 7\times10^{16}$ ions/cm^2) display the more usually observed Mott VRH model. For the higher dosage samples ($\varphi \geqslant 10^{17}$ ions/cm^2), the σ_{RT} increases further with a dramatic change in the temperature dependence which fits to a model with weak localization and electron-electron interaction effects dominating the charge transport. The fitting of the conductivity results from this model indicates a dimensional crossover for the WL effect at $\sim$40–50 K. It is concluded that a 3D interconnected carbon network reforms upon ion implantation on these densely packed polymer samples. At higher dosages, the implantation creates a sp^2 carbon rich network which is responsible for the semimetallic behavior; and at lower dosages, the system still contains noncarbon atoms as shown in the XPS spectra, which results in a more localized state and a 3D hopping conduction in these samples.

ACKNOWLEDGMENTS

This work was supported in part by Air Force OSR Grant No. F49620-92-C0002, the National Science Foundation Grant No. DMR-9508723, and the Office of Naval Research.

*Present address: Lake Shore Electronics, Inc., 575 McCorkle Blvd., Westerville, OH 43082.

†Present address: Department of Chemistry, Kent State University-Stark Campus, 6000 Frank Avenue, Canton, OH 44720.

‡Present address: Department of Physics, Korea University, Seoul 136-701, Korea.

[1] J. Robertson, Adv. Phys. **35**, 317 (1986); J. Robertson and E. P. O'Reilly, Phys. Rev. B **35**, 2946 (1987).

[2] D. F. Baker and R. H. Bragg, Phys. Rev. B **28**, 2219 (1983).

[3] P. Bätz, D. Schmeisser, I. Belaish, D. Davidov, and W. Göpel, Synth. Met. **42**, 1609 (1991); J. I. Jin, J. H. Kim, Y. H. Lee, G. H. Lee, and Y. W. Park, *ibid.* **57**, 3742 (1993).

[4] T. Venkatesan, L. Calcagno, B. S. Elman, and G. Foti, in *Ion Beam Modification Insulators*, edited by P. Mazzoldi and G. W. Arnold (Elsevier, Amsterdam, 1987), p. 301.

[5] M. L. Kaplan, S. R. Forrest, P. H. Schmidt, and T. Venkatesen, J. Appl. Phys. **55**, 732 (1984).

[6] M. S. Dresselhaus and R. Kalish, *Ion Implantation in Diamond, Graphite, and Related Materials* (Springer-Verlag, Berlin, 1992), Vol. 22.

[7] A. Burns, Z. H. Wang, G. Du, J. Joo, J. A. Osaheni, S. A. Jenekhe, C. S. Wang, and A. J. Epstein, in *Electrical, Optical, and Magnetic Properties of Organic Solid State Materials*, edited by L. Y. Chiang, A. F. Garito, and D. J. Sandman (Materials Research Society, Pittsburgh, 1992), Vol. 247, p. 735.

[8] B. S. Elman, D. J. Sandman, and M. A. Newkirk, Appl. Phys. Lett. **46**, 100 (1985).

[9] B. I. Shklovskii and A. L. Efros, *Electronic Properties of Semiconductors* (Springer-Verlag, Berlin, 1984), Vol. 45; D. Belitz and T. R. Kirkpatrick, Rev. Mod. Phys. **66**, 261 (1994).

[10] G. Du, V. N. Prigodin, A. Burns, J. Joo, C. S. Wang, and A. J. Epstein, Phys. Rev. B **58**, 4485 (1998).

[11] B. S. Elman, M. S. Dresselhaus, G. Dresselhaus, E. W. Maby, and H. Mazurek, Phys. Rev. B **24**, 1027 (1981).

[12] J. Robertson, Adv. Phys. **35**, 317 (1986); J. Robertson and E. P. O'Reilly, Phys. Rev. B **35**, 2946 (1987).

[13] S. Kobayashi and F. Komori, Prog. Theor. Phys. Suppl. **84**, 224 (1985).

[14] B. L. Altshuler and A. G. Aronov, in *Electron-Electron Interactions in Disordered Systems*, edited by A. L. Efros and M. Pollak (North-Holland, Amsterdam, 1985), p. 1; P. A. Lee and T. V. Ramakrishnan, Rev. Mod. Phys. **57**, 287 (1985).

[15] S. A. Jenekhe and P. O. Johnson, Macromolecules **23**, 4419 (1990); S. A. Jenekhe and S. J. Tibbetts, J. Polym. Sci., Part B: Polym. Phys. **26**, 201 (1988); J. F. Wolfe and F. E. Arnold, Macromolecules **14**, 909 (1981).

[16] A. G. Zabrodskii and K. N. Zinov'eva, Sov. Phys. JETP **59**, 425 (1984).

[17] N. F. Mott and E. Davis, *Electronic Processes in Non-Crystalline Materials* (Clarendon, Oxford, 1979).

[18] J. A. Osaheni, S. A. Jenekhe, A. Burns, G. Du, J. Joo, Z. Wang, and A. J. Epstein, Macromolecules **25**, 5828 (1992).

[19] I. M. Lifshitz, S. A. Gredeskul, and L. A. Pastur, *Introduction to the Disordered Systems* (Wiley, New York, 1988).

[20] G. A. Thomas, A. Kawabata, Y. Ootuka, S. Katsumoto, S. Kobayashi, and W. Sasaki, Phys. Rev. B **26**, 2113 (1982).

[21] R. F. Milligan, T. F. Rosenbaum, R. N. Bhatt, and G. A. Thomas, in *Electron-Electron Interactions in Disordered Systems*, edited by A. J. Efros and M. Pollak (North-Holland, Amsterdam, 1985), p. 231.

[22] G. Bergmann, Phys. Rep. **107**, 1 (1984).

[23] A. Möbius, J. Phys. C **18**, 4639 (1985).

[24] J. W. Mayer , L. Eriksson, and J. A. Davies, *Ion Implantation of Semiconductors, Silicon, and Germanium* (Academic, New York, 1970); G. Carter and W. A. Grant, *Ion Implantation of Semiconductors* (Arnold, London, 1976).

[25] H. H. Song and C. S. Wang, Polymer **34**, 4793 (1993).

[26] H. H. Song, A. V. Fratini, M. Chabinyc, G. E. Price, A. K. Agrawal, C. S. Wang, D. S. Dudis, and F. E. Arnold, Synth. Met. **69**, 533 (1995).